IEEE Access
Multidisciplinary | Rapid Review | Open Access Journal

Received April 8, 2021, accepted April 16, 2021, date of publication April 26, 2021, date of current version May 12, 2021.

Digital Object Identifier 10.1109/ACCESS.2021.3075564

Adaptive Sliding Mode Control for Spacecraft Rendezvous With Unknown System Parameters and Input Saturation

ZONGLING LI[1,2], GANXIN YU[4], QINGJUN ZHANG[2], SHUO SONG[3], AND HONGTAO CUI[4]

[1]School of Information and Electronics, Beijing Institute of Technology, Beijing 100081, China
[2]Institute of Spacecraft System Engineering, China Academy of Space Technology, Beijing 100094, China
[3]School of Automation, Harbin Engineering University, Harbin 150001, China
[4]College of Aerospace and Civil Engineering, Harbin Engineering University, Harbin 150001, China

Corresponding author: Shuo Song (ss320047105@hrbeu.edu.cn)

This work was supported in part by the National Natural Science Foundation of China under Grant 11772185, in part by the Natural Science Foundation of Heilongjiang Province under Grant F2017005, in part by the Project under Grant D020214, and in part the Joint Laboratory of Integrated Dynamics and Control for Spacecraft, the Joint Laboratory of Space Guidance and Control Technology.

ABSTRACT In this study, we investigated the sliding mode control (SMC) for the spacecraft rendezvous maneuver under unknown system parameters and input saturations. On the basis of the attitude and position tracking subsystem, two anti-saturation sliding mode surfaces (SMSs) are constructed to guarantee the exponential convergence of tracking errors between the target spacecraft and the pursuer spacecraft. In connection with hyperbolic tangent, a modified auxiliary system is established to compensate the nonlinear constraint caused by the actuator saturation. Meanwhile, in order to enhance the practicability and reliability of the controller, unknown inertial information is taken into consideration. The resulting system uncertainties are estimated accurately via adaptive laws. Additionally, it is concluded that the designed controller is capable of ensuring the boundedness of the closed-loop signals with reasonable selection of control parameters. Finally, the effectiveness and advantages of the proposed methods are verified through numerical simulations.

INDEX TERMS Spacecraft rendezvous maneuver, asymptotic tracking control, sliding mode control, input saturation, adaptive control.

I. INTRODUCTION

In the last several decades, the rendezvous maneuver control of spacecraft has been widely applied in space missions such as construction of orbiting space stations, docking and removing space debris, among others. Furthermore, the adequate tracking accuracy and anti-disturbance capability of controller are essential requirements for outer-space missions. Considering the external disturbance, actuator saturation, parameter uncertainty and other factors, the design of rendezvous maneuver controller for spacecraft becomes more challenging. Through protracted and unremitting efforts, some scientific methods have aroused great research interest for spacecraft tracking control in recent years, such as adaptive control [1], [2], backstepping control [3]–[5], neural network-based control [5], [6], fault-tolerant control [7]–[9] as well as SMC [10], [11].

The associate editor coordinating the review of this manuscript and approving it for publication was Zheng Chen.

For specific aspect of the spacecraft tracking and synchronization control, the spacecraft in space orbit will be affected by a variety of environmental torques and internal action, and all these interfering forces are usually uncertain. It is impossible to make an accurate observation for all this information, which is called non-parametric uncertainty. In order to improve the control precision for nonlinear systems, the problem of suppressing the disturbing moment must be considered in the tracking controllers [12]. In particular, the disturbance observer-based control is an effective tool to handle model uncertainties. In [13], an extended state observer (ESO) is constructed to reach high tracking performance. Attributing to the desirable approximation capability for uncertainties, the neural networks (NNs) are employed into tracking controller design [14], [15]. However, take account into the utilization of NNs will consume large computation energy, the sliding mode control (SMC) is introduced [16] for the ability of anti-disturbance, easy implement and low computation consumption. It should be noted that

none of the above literatures consider collision avoidance for rendezvous maneuver control, so that it is likely to cause serious space accidents. In addition, the space debris has increased dramatically which will pose a significant threat to the safety of spacecraft missions. Therefore, artificial potential function-based backstepping control has been presented in [17] to improve the collision avoidance ability of the system.

A common disadvantage in above results is that they depend on the availability of the inertial parameters. However, inertial parameters are not always measured definitely for designers during practical missions, for which actions like fuel consumption, rendezvous and docking between space vehicles, load and shape adjustments, will change the inertial information of in-orbit spacecrafts [18]–[20]. Given this fact, with no exact knowledge for the mass and inertial matrix of control object, an extended state observer is designed in [18] to estimate the relative parameters in real-time. By using the obtained estimates, a backstepping-based robust finite-time controller is proposed to achieve attitude tracking control for the rigid spacecraft. As a technical extension of this result, an adaptive control algorithm based on neural networks is constructed in [19], where the uncertainties and external disturbances are addressed to guarantee the robustness under harsh environments. To further improve the approximation precision for the unknown nonlinear dynamic, an adaptive relative position controller is designed in [20], so that the rendezvous and proximity maneuvers are achieved in virtue of a comprehensive adaptive fuzzy strategy.

Despite the helpful results mentioned above, the rendezvous maneuver control for spacecrafts still poses the considering caveat of actuator saturations. On account of physical structure and energy consumption, there does exist an upper limit for the output thrust of actuators. This phenomenon results in that the desired control signal is maybe executed unerringly. To prevent the performance attenuation and unreliable hazard caused by the nonlinearity, a significant amount of anti-saturation control algorithms are exploited in combination with various innovational operating patterns [21]–[24]. In [21], a novel dead-zone operator-based model is introduced for spacecraft fly-around in presence of input saturation. Subsequently, the convergence rate of this result is further optimized in [22]. Guo *et al.* utilized a modified terminal sliding mode to accomplish the finite-time anti-unwinding control in the case of saturation constraint. In [23], this method is further extended to the context that unknown actuator fault occurs. Meanwhile, the radial basis function neural network (RBFNN) nonlinear approximation surmounts the uncertain dynamics in inaccurate model.

Motivated by the above observations, this study addresses the rendezvous maneuver control for rigid spacecrafts and takes account of the actuator saturations and parameter uncertainties synchronously. A hyperbolic tangent-based terminal sliding mode surface (TSMS) is constructed to guarantee the stabilization of relative errors, while system uncertainties are handled by resorting to elaborate adaptive laws. Meanwhile, a modified auxiliary system is established to compensate the saturation nonlinearity effectively. The contributions of this paper are as follows:

i) Hyperbolic tangent-based auxiliary system is developed to cope with the saturation characteristic of actuators. Different from the solutions in [14], [15] which depends on part of the mode parameters' information, a mode-free method is introduced in this paper to overcome this drawback. In this way, the anti-saturation control scheme can be more applicable in practical implement.

ii) The designed controller has the ability of preventing chattering. With the increase of parameter ε, the chattering will decrease but the tracking performance will also degrade. This paper makes a trade-off between the chattering and tracking performance. Compared with the existing control schemes of spacecraft rendezvous maneuver [7], [11], [25], the time-varying inertial parameters are considered in this paper, and the resulting unavailable dynamics are estimated by the design of adaptive update laws.

The remainder of this paper is arranged as follows. The dynamics model of the spacecraft is established in Section 2. Subsequently, two controllers are described in Section 3 and the effectiveness of the controller is proved through simulations in Section 4. Finally, the conclusion of this paper is given in Section 5.

II. SPACECRAFT MODEL AND PRELIMINARIES

A. RELATIVE ATTITUDE DYNAMIC MODEL

For the purpose of ensuring singular-free property, the attitude dynamics for rigid spacecrafts are described via the adoption of unit quaternion. In this connection, the rotation matrix $\boldsymbol{R} \in SO(3)$ and the unit quaternion $\boldsymbol{Q} = \left[q_0, \boldsymbol{q}_v^{\mathrm{T}}\right]^{\mathrm{T}} \in \Xi$ with $\Xi = \left\{\boldsymbol{Q} \in \mathbb{R} \times \mathbb{R}^{3\times 3} \,\middle|\, q_0^2 + \boldsymbol{q}_v^{\mathrm{T}}\boldsymbol{q}_v = 1\right\}$ are introduced for model formulation. Hence, the attitude parameters of the pursuer and target are denoted as $\boldsymbol{Q}_p$ and $\boldsymbol{Q}_t$, respectively. Afterwards, it is defined that $\tilde{\boldsymbol{Q}}$ is the relative attitude between pursuer and target, which is given as:

$$\tilde{\boldsymbol{Q}} = \left[\tilde{q}_0, \tilde{\boldsymbol{q}}_v^{\mathrm{T}}\right]^{\mathrm{T}} = \mathbf{Q}_t^{-1} \odot \mathbf{Q}_p \tag{1}$$

where the denotation $\odot$ stands for the unit quaternion product. According to the theory in [26], the relative attitude kinematics can be written as:

$$\dot{\tilde{q}}_0 = -\frac{1}{2}\tilde{\boldsymbol{q}}_v^{\mathrm{T}}\tilde{\boldsymbol{\omega}} \tag{2}$$

$$\dot{\tilde{\boldsymbol{q}}}_v = \frac{1}{2}\left(\tilde{\boldsymbol{q}}_v^{\times} + \tilde{q}_0\boldsymbol{I}_3\right)\tilde{\boldsymbol{\omega}} \tag{3}$$

where the relative angular velocity $\tilde{\boldsymbol{\omega}}$ can be defined as $\tilde{\boldsymbol{\omega}} = \boldsymbol{\omega}_p - \tilde{\boldsymbol{R}}\boldsymbol{\omega}_t$; $\boldsymbol{\omega}_p$ and $\boldsymbol{\omega}_t$ represent the angular velocity of the pursuer and the target separately.

With $\boldsymbol{J}_t \in \mathbb{R}^{3\times 3}$ and $\boldsymbol{J} \in \mathbb{R}^{3\times 3}$ being the inertia matrixes of the target and pursuer, respectively, the following result can be concluded:

$$\boldsymbol{J}\dot{\tilde{\boldsymbol{\omega}}} = -\boldsymbol{C}_r\tilde{\boldsymbol{\omega}} - \boldsymbol{n}_r + \boldsymbol{\tau} + \boldsymbol{\tau}_d \tag{4}$$

where $\boldsymbol{C}_r = \boldsymbol{J}\left(\tilde{\boldsymbol{R}}\boldsymbol{\omega}_t\right)^{\times} + \left(\tilde{\boldsymbol{R}}\boldsymbol{\omega}_t\right)^{\times}\boldsymbol{J} - \left(\boldsymbol{J}\left(\tilde{\boldsymbol{\omega}} + \tilde{\boldsymbol{R}}\boldsymbol{\omega}_t\right)\right)^{\times}$ and $\boldsymbol{n}_r = \left(\tilde{\boldsymbol{R}}\boldsymbol{\omega}_t\right)^{\times}\boldsymbol{J}\tilde{\boldsymbol{R}}\boldsymbol{\omega}_t + \boldsymbol{J}\dot{\tilde{\boldsymbol{R}}}\boldsymbol{\omega}_t$. The control torque and the influence of external disturbance are recorded as $\boldsymbol{\tau} \in \mathbb{R}^3$ and $\boldsymbol{\tau}_d \in \mathbb{R}^3$, respectively. More details on the modeling of attitude dynamics can be found in Ref. [1]

B. RELATIVE ORBIT DYNAMICS MODEL

Upon the utilization of the relation of the relative motion, the pursuer's position and velocity are denoted as $\boldsymbol{r}_p$ and $\boldsymbol{v}_p$, whose descriptions are exhibited in Eqs. (5)-(6).

$$\boldsymbol{r}_p = \tilde{\boldsymbol{r}} + \tilde{\boldsymbol{R}}\left(\boldsymbol{r}_t + \boldsymbol{\sigma}_t\right) \tag{5}$$

$$\boldsymbol{v}_p = \tilde{\boldsymbol{v}} + \tilde{\boldsymbol{R}}\left(\boldsymbol{v}_t + \boldsymbol{\omega}_t^{\times}\boldsymbol{\sigma}_t\right) \tag{6}$$

Here, $\boldsymbol{r}_t$ and $\boldsymbol{v}_t$ are the target's position and velocity; $\tilde{\boldsymbol{r}}$ and $\tilde{\boldsymbol{v}}$ represent the relative position and velocity, respectively; $\boldsymbol{\sigma}_t \in \mathbb{R}^3$ means a constant vector denoting the desired rendezvous position. The derivative of Eq. (5) can be obtained as:

$$\dot{\tilde{\boldsymbol{r}}} = \tilde{\boldsymbol{v}} - \boldsymbol{C}_t\tilde{\boldsymbol{r}} \tag{7}$$

where $\boldsymbol{C}_t = \left(\tilde{\boldsymbol{\omega}} + \tilde{\boldsymbol{R}}\boldsymbol{\omega}_t\right)^{\times}$. Consequently, it can be computed the derivative of Eq. (7) as:

$$\dot{\boldsymbol{v}}_p = \dot{\tilde{\boldsymbol{v}}} + \dot{\tilde{\boldsymbol{R}}}\left(\boldsymbol{v}_t + \boldsymbol{\omega}_t^{\times}\boldsymbol{\sigma}_t\right) + \tilde{\boldsymbol{R}}\left(\dot{\boldsymbol{v}}_t + \dot{\boldsymbol{\omega}}_t^{\times}\boldsymbol{\sigma}_t\right) \tag{8}$$

Based on the idea of simplicity, the foregoing relation can be rewritten as:

$$m_p\dot{\tilde{\boldsymbol{v}}} = -m_p\boldsymbol{C}_t\tilde{\boldsymbol{v}} - m_p\boldsymbol{n}_t + \boldsymbol{f} + \boldsymbol{f}_d \tag{9}$$

where $\boldsymbol{n}_t = \left(\tilde{\boldsymbol{R}}\boldsymbol{\omega}_t\right)^{\times}\tilde{\boldsymbol{R}}\boldsymbol{v}_t + \tilde{\boldsymbol{R}}\dot{\boldsymbol{v}}_t + \tilde{\boldsymbol{\omega}}^{\times}\tilde{\boldsymbol{R}}\boldsymbol{\sigma}_t^{\times}\boldsymbol{\omega}_t - \tilde{\boldsymbol{R}}\boldsymbol{\sigma}_t^{\times}\dot{\boldsymbol{\omega}}_t$. m_t and m_p are defined as the masses of the target and the purser; $\boldsymbol{f} \in \mathbb{R}^3$ and $\boldsymbol{f}_d \in \mathbb{R}^3$ stand for the control torque and external impacts, respectively.

C. PROBLEM FORMULATION

To convenient matter, choose $\boldsymbol{\varepsilon}_r$, $\boldsymbol{\varepsilon}_t$, $\boldsymbol{d}_r$ and $\boldsymbol{d}_t$ to replace the control torques and disturbance toques, i.e.:

$$\begin{aligned} \boldsymbol{\varepsilon}_r &= \boldsymbol{\tau}, \quad \boldsymbol{\varepsilon}_t = \boldsymbol{f} \\ \boldsymbol{d}_r &= \boldsymbol{\tau}_d, \quad \boldsymbol{d}_t = \boldsymbol{f}_d \end{aligned} \tag{10}$$

where $\boldsymbol{\varepsilon}_r$, $\boldsymbol{\varepsilon}_t$ are yet to be designed in the following.

Integrating Eq. (4), (9)-(10) and in view of the actuator constraint, the relative dynamics between target and purser can be established as:

$$\boldsymbol{J}\dot{\tilde{\boldsymbol{\omega}}} = -\boldsymbol{C}_r\tilde{\boldsymbol{\omega}} - \boldsymbol{n}_r + \boldsymbol{u}\left(\boldsymbol{\varepsilon}_r\right) + \boldsymbol{d}_r \tag{11}$$

$$m\dot{\tilde{\boldsymbol{v}}} = -m\boldsymbol{C}_t\tilde{\boldsymbol{v}} - m\boldsymbol{n}_t + \boldsymbol{u}\left(\boldsymbol{\varepsilon}_t\right) + \boldsymbol{d}_t \tag{12}$$

In particular, the nonlinearity of saturation is expressed as:

$$\begin{aligned} \boldsymbol{u}\left(\boldsymbol{\varepsilon}\right) &= \left[u\left(\varepsilon_1\right), u\left(\varepsilon_2\right), u\left(\varepsilon_3\right)\right]^{\mathbf{T}} \\ u\left(\varepsilon_i\right) &= \mathrm{sat}\left(\varepsilon_i\right) = \begin{cases} \mathrm{sign}\left(\varepsilon_i\right)u_M, & \varepsilon_i \geq u_M \\ \varepsilon_i, & \varepsilon_i < u_M \end{cases}, i = 1, 2, 3 \end{aligned} \tag{13}$$

where $\boldsymbol{\varepsilon} \in \mathbb{R}^{3\times 3}$ is the normal input torque and u_M is the upper bound of the actuators.

Remark 1: From the practical perspective, the characteristic of actuator saturation is extensively existent in control engineering for the general in-orbit spacecraft. Due to the structural limitation of mechanical and pneumatic components, the actuator has no capability to output an infinite control torque. This condition is considered as a new challenge for the controller design of spacecraft rendezvous maneuver. If the upper limit of the torque provided by the actuator is ignored, the control accuracy will inevitably suffer from unpredictable adverse effects and even threaten the stability of the closed-loop system. For this case, this paper constructs a novel anti-saturation auxiliary system to compensate the restriction.

Remark 2: Numerous existing literatures regard the inertial parameters and mass of spacecrafts as known qualities, which does not conform to the practical engineering scenario, however. Due to the consumption of fuel or propellant, as well as the deformations caused by mission requirements, the mass and inertia matrix of the spacecraft are in a state of slow flux. It is undoubtedly necessary to adapt the design of controller for this change.

Assumption 1: The dynamics of the target is stable, i.e., $\boldsymbol{\omega}_t$, $\boldsymbol{v}_t$, and $\dot{\boldsymbol{v}}_t$ are bounded reference information satisfying $\|\boldsymbol{\omega}_t\| \leq a_1$, $\|\dot{\boldsymbol{\omega}}_t\| \leq a_2$, $\|\boldsymbol{v}_t\| \leq a_3$, and $\|\dot{\boldsymbol{v}}_t\| \leq a_4$, where a_1, a_2, a_3, and a_4 are all unknown positive constants.

Assumption 2: The inertia parameters $\boldsymbol{J}$ and m are both uncertain bounded variables with $\|\boldsymbol{J}\| \leq b_1$, $\left\|\dot{\boldsymbol{J}}\right\| \leq b_2$, $m \leq b_3$, and $|\dot{m}| \leq b_4$, where b_1, b_2, b_3, and b_4 are all unknown positive constants.

Assumption 3: The environmental disturbances $\boldsymbol{d}_r$ and $\boldsymbol{d}_t$ are unavailable bounded vectors satisfying $\|\boldsymbol{d}_r\| \leq D_1$ and $\|\boldsymbol{d}_t\| \leq D_2$, where both D_1 and D_2 are unknown positive constants.

Lemma 1 ([1]): For a variable $x \in \mathbb{R}$, the hyperbolic tangent function satisfies the inequation of $0 < |x| - x\tanh(\mu x) \leq \frac{\delta}{\mu}$ with $\mu > 0$ and $\delta = 0.2785$.

Lemma 2 ([31]): For any positive constants α and β, the following relation holds:

$$0 \leq |\alpha| - \frac{|\alpha|^2}{\sqrt{\alpha^2 + \beta^2}} \leq |\alpha| - \frac{|\alpha|^2}{|\alpha| + \beta} < \beta \tag{14}$$

D. CONTROL OBJECTIVE

The control objective of this work can be stated as follows. Under the condition that the motion information of the target spacecraft can be obtained by the pursuer, the designed control inputs $\boldsymbol{\varepsilon}_r$, $\boldsymbol{\varepsilon}_t$ are capable of facilitating the pursuer to complete the attitude and orbit tracking, so that the rendezvous and docking mission can be realized in space.

III. CONTROL DESIGN

For the purpose of achieving the trajectory tracking of the pursuer to the target, two continuous adaptive anti-saturation sliding mode controllers are constructed for the subsystems

of attitude and position, respectively. In consideration of the system uncertainties arising from the time-varying inertial parameters, adaptive estimation is applied to approximate the nonlinear dynamics. Meanwhile, the input constraint caused by actuator saturation is compensated steadily by resorting to a modified auxiliary framework. Consequently, Lyapunov-based analysis guarantees the exponential convergence of tracking errors.

For the purpose of the attitude and orbit tracking control for the pursuer, two anti-saturation continues SMS are constructed as:

$$\boldsymbol{s}_1 = \tilde{\boldsymbol{\omega}} + k_1\tilde{\boldsymbol{q}}_v - k_2\tanh\left(\boldsymbol{\chi}_1\right) \tag{15}$$

$$\boldsymbol{s}_2 = \tilde{\boldsymbol{v}} + k_5\tilde{\boldsymbol{r}} - k_6\tanh\left(\boldsymbol{\chi}_2\right) \tag{16}$$

where $k_1 > \frac{1}{2}$ and $k_5 > \frac{1}{2} - \|\boldsymbol{C}_t\|$ with k_2 and k_6 being positive constants, $\boldsymbol{\chi}_1$ and $\boldsymbol{\chi}_2$ are two dynamic vectors defined as follows:

$$\begin{aligned}\dot{\boldsymbol{\chi}}_1 &= \frac{\boldsymbol{\varphi}_1^{-1}\boldsymbol{J}^{-1}}{k_2}\left[-\kappa_1\tanh\left(\boldsymbol{\chi}_1\right) + \mathrm{sat}\left(\boldsymbol{\varepsilon}_r\right) - \boldsymbol{\varepsilon}_r\right],\\ \boldsymbol{\chi}_1(0) &= \boldsymbol{0}\end{aligned} \tag{17}$$

$$\begin{aligned}\dot{\boldsymbol{\chi}}_2 &= \frac{\boldsymbol{\varphi}_2^{-1}}{k_6 m}\left[-\kappa_2\tanh\left(\boldsymbol{\chi}_2\right) + \mathrm{sat}\left(\boldsymbol{\varepsilon}_t\right) - \boldsymbol{\varepsilon}_t\right],\\ \boldsymbol{\chi}_2(0) &= \boldsymbol{0}\end{aligned} \tag{18}$$

with the constants $\kappa_1 > 0$, $\kappa_2 > 0$ and $\boldsymbol{\varphi}_1 = diag\left[1-\tanh^2(\chi_{11}), 1-\tanh^2(\chi_{12}), 1-\tanh^2(\chi_{13})\right]$, $\boldsymbol{\varphi}_2 = \mathrm{diag}\left[1-\tanh^2(\chi_{21}), 1-\tanh^2(\chi_{22}), 1-\tanh^2(\chi_{23})\right]$, where $\boldsymbol{\varphi}_1$ and $\boldsymbol{\varphi}_2$ are nonsingular to guarantee the definitions true.

Remark 3: In the reference [29], the presented method can guarantee asymptotic tracking performance with zero steady-state error, which will effectively improve the control accuracy. Different from this kind of control approach, an anti-saturation auxiliary system is constructed in this paper. This is the most valuable contribution of this paper. For the anti-saturation auxiliary system $\dot{\chi} = -\zeta\chi + \mathrm{sat}(u) - u$ presented in [28], it has the capability of surmounting system nonlinearity caused by input saturation effectively. However, the auxiliary variable χ must be assumed to be bounded. To relax the restraint, the hyperbolic tangent function is employed here for the error transformation.

In terms of Eqs. (3)-(4), (11)-(12) and (15)-(16), the derivative of $\boldsymbol{s}_1$ and $\boldsymbol{s}_2$ can be calculated as:

$$\begin{aligned}\boldsymbol{J}\dot{\boldsymbol{s}}_1 &= \boldsymbol{J}\dot{\tilde{\boldsymbol{\omega}}} + k_1\boldsymbol{J}\dot{\tilde{\boldsymbol{q}}}_v - k_2\boldsymbol{J}\boldsymbol{\varphi}_1\dot{\boldsymbol{\chi}}_1\\ &= -\boldsymbol{C}_r\tilde{\boldsymbol{\omega}} - \boldsymbol{n}_r + \mathrm{sat}\left(\boldsymbol{\varepsilon}_r\right) + \boldsymbol{d}_r + \frac{k_1}{2}\boldsymbol{J}\left(\tilde{\boldsymbol{q}}_v^{\times} + \tilde{q}_0\boldsymbol{I}_3\right)\tilde{\boldsymbol{\omega}}\\ &\quad + \kappa_1\tanh\left(\boldsymbol{\chi}_1\right) - \mathrm{sat}\left(\boldsymbol{\varepsilon}_r\right) + \boldsymbol{\varepsilon}_r\\ &= \boldsymbol{\varepsilon}_r - \boldsymbol{C}_r\tilde{\boldsymbol{\omega}} - \boldsymbol{n}_r + \boldsymbol{d}_r + \frac{k_1}{2}\boldsymbol{J}\left(\tilde{\boldsymbol{q}}_v^{\times} + \tilde{q}_0\boldsymbol{I}_3\right)\tilde{\boldsymbol{\omega}}\\ &\quad + \kappa_1\tanh\left(\boldsymbol{\chi}_1\right)\end{aligned} \tag{19}$$

$$\begin{aligned}m\dot{\boldsymbol{s}}_2 &= m\dot{\tilde{\boldsymbol{v}}} + k_5 m\dot{\tilde{\boldsymbol{r}}} - k_6 m\boldsymbol{\varphi}_2\dot{\boldsymbol{\chi}}_2\\ &= -m\boldsymbol{C}_t\tilde{\boldsymbol{v}} - m\boldsymbol{n}_t + \mathrm{sat}\left(\boldsymbol{\varepsilon}_t\right) + \boldsymbol{d}_t + k_5 m\dot{\tilde{\boldsymbol{r}}}\\ &\quad + \left(\kappa_2\tanh\left(\boldsymbol{\chi}_2\right) - \mathrm{sat}\left(\boldsymbol{\varepsilon}_t\right) + \boldsymbol{\varepsilon}_t\right)\\ &= \boldsymbol{\varepsilon}_t - m\boldsymbol{C}_t\tilde{\boldsymbol{v}} - m\boldsymbol{n}_t + \boldsymbol{d}_t + k_5 m\dot{\tilde{\boldsymbol{r}}} + \kappa_2\tanh\left(\boldsymbol{\chi}_2\right)\end{aligned} \tag{20}$$

Remark 4: In consideration of Assumptions 1–3, it is concluded that $\left\|\tilde{\boldsymbol{R}}\right\| = 1$, $\left\|\tilde{\boldsymbol{q}}_v^{\times} + \tilde{q}_0\boldsymbol{I}_3\right\| = 1$, $\|-\boldsymbol{C}_r\tilde{\boldsymbol{\omega}}\| = \left\|-\left(\boldsymbol{J}\left(\tilde{\boldsymbol{R}}\boldsymbol{\omega}_t\right)^{\times} + \left(\tilde{\boldsymbol{R}}\boldsymbol{\omega}_t\right)^{\times}\boldsymbol{J} - \left(\boldsymbol{J}\left(\tilde{\boldsymbol{\omega}} + \tilde{\boldsymbol{R}}\boldsymbol{\omega}_t\right)\right)^{\times}\right)\tilde{\boldsymbol{\omega}}\right\| \le \left\|-2\boldsymbol{J}\boldsymbol{\omega}_t\tilde{\boldsymbol{\omega}} + \boldsymbol{J}\tilde{\boldsymbol{\omega}}^2 + \boldsymbol{\omega}_t\tilde{\boldsymbol{\omega}}\right\| \le a_1 b_1\|\tilde{\boldsymbol{\omega}}\| + b_1 \times \|\tilde{\boldsymbol{\omega}}\|^2$, $\|-\boldsymbol{n}_r\| = \left\|\left(\tilde{\boldsymbol{R}}\boldsymbol{\omega}_t\right)^{\times}\boldsymbol{J}\tilde{\boldsymbol{R}}\boldsymbol{\omega}_t + \boldsymbol{J}\tilde{\boldsymbol{R}}\dot{\boldsymbol{\omega}}_t\right\| = \left\|-\boldsymbol{J}\boldsymbol{\omega}_t^2 - \boldsymbol{J}\dot{\boldsymbol{\omega}}_t\right\| \le a_1^2 b_1 + b_1 a_2$, $\left\|\frac{k_1}{2}\boldsymbol{J}\left(\tilde{\boldsymbol{q}}_v^{\times} + \tilde{q}_0\boldsymbol{I}_3\right)\tilde{\boldsymbol{\omega}}\right\| \le \left\|\frac{k_1}{2}\boldsymbol{J}\tilde{\boldsymbol{\omega}}\right\| \le \frac{1}{2}k_1 b_1\|\tilde{\boldsymbol{\omega}}\|$.

Remark 5: According to Assumptions 1-3, it can be concluded that $\|-m\boldsymbol{C}_t\tilde{\boldsymbol{v}}\| = \left\|-m\left(\tilde{\boldsymbol{\omega}} + \tilde{\boldsymbol{R}}\boldsymbol{\omega}_t\right)^{\times}\tilde{\boldsymbol{v}}\right\| \le b_3\|\tilde{\boldsymbol{\omega}}\|\|\tilde{\boldsymbol{v}}\| + b_3 a_1\|\tilde{\boldsymbol{v}}\|$, $\|-m\boldsymbol{n}_t\| = \left\|-m\left(\left(\tilde{\boldsymbol{R}}\boldsymbol{\omega}_t\right)^{\times}\tilde{\boldsymbol{R}}v_t + \tilde{R}\dot{v}_t + \tilde{\boldsymbol{\omega}}^{\times}\tilde{\boldsymbol{R}}\tilde{\sigma}_t^{\times}\boldsymbol{\omega}_t\ \sigma_t^{\times}\dot{\boldsymbol{\omega}}_t\right)\right\| \le b_3 a_1 a_3 + b_3 a_4 + b_3\|\boldsymbol{\delta}_t\|\|a_1\|\|\tilde{\boldsymbol{\omega}}\| + b_3\|\boldsymbol{\delta}_t\|a_2$, $\left\|k_5 m\dot{\tilde{\boldsymbol{r}}}\right\| \le k_5 b_3\|\tilde{v}\| + k_5 b_3\|\tilde{\boldsymbol{\omega}}\|\|\tilde{r}\| + k_5 b_3 a_1\|\tilde{r}\|$.

On the basis of Remark 4 and Remark 5, it can be derived the following inequalities:

$$\begin{aligned}&\left\|-\boldsymbol{C}_r\tilde{\boldsymbol{\omega}} - \boldsymbol{n}_r + \boldsymbol{d}_r + \frac{k_1}{2}\boldsymbol{J}\left(\tilde{\boldsymbol{q}}_v^{\times} + \tilde{q}_0\boldsymbol{I}_3\right)\tilde{\boldsymbol{\omega}} + \kappa_1\tanh\left(\boldsymbol{\chi}_1\right)\right\|\\ &\quad \le \alpha_1\|\tilde{\boldsymbol{\omega}}\|^2 + \alpha_2\|\tilde{\boldsymbol{\omega}}\| + \alpha_3\end{aligned} \tag{21}$$

$$\begin{aligned}&\left\|-m\boldsymbol{C}_t\tilde{\boldsymbol{v}} - m\boldsymbol{n}_t + \boldsymbol{d}_t + k_5 m\dot{\tilde{\boldsymbol{r}}} + \kappa_2\tanh\left(\boldsymbol{\chi}_2\right)\right\|\\ &\quad \le \alpha_4\|\tilde{\boldsymbol{\omega}}\|\|\tilde{\boldsymbol{v}}\| + \alpha_5\|\tilde{\boldsymbol{\omega}}\|\|\tilde{\boldsymbol{r}}\| + \alpha_6\|\tilde{\boldsymbol{\omega}}\| + \alpha_7\|\tilde{\boldsymbol{v}}\|\\ &\qquad + \alpha_8\|\tilde{\boldsymbol{r}}\| + \alpha_9\end{aligned} \tag{22}$$

where $\alpha_i\,(i = 1, 2, 3, 4, 5, 6, 7, 8, 9)$ are unknown positive constants and satisfy $\alpha_1 = b_1$, $\alpha_2 = \frac{1}{2}k_1 b_1 + a_1 b_1$, $\alpha_3 = a_1^2 b_1 + b_1 a_2 + D_1 + \sqrt{3}\kappa_1$, $\alpha_4 = b_3$, $\alpha_5 = k_5 b_3$, $\alpha_6 = b_3\|\boldsymbol{\delta}_t\| \times \|a_1\|$, $\alpha_7 = k_5 b_3 + b_3 a_1$, $\alpha_8 = k_5 b_3 a_1$, $\alpha_9 = b_3\|\boldsymbol{\delta}_t\|a_2 + b_3 a_1 a_3 + b_3 a_4 + D_2 + \sqrt{3}\kappa_2$.

It is defined that $\hat{\alpha}_i\,(i = 1, 2, 3, 4, 5, 6, 7, 8, 9)$ are the estimated values of $\alpha_i\,(i = 1, 2, 3, 4, 5, 6, 7, 8, 9)$. Hence, the control signals for attitude and orbit tracking control systems are designed as:

$$\begin{aligned}\boldsymbol{\varepsilon}_r &= -\frac{\boldsymbol{s}_1\hat{\alpha}_1^2\|\tilde{\boldsymbol{\omega}}\|^4}{\sqrt{\|\boldsymbol{s}_1\|^2\hat{\alpha}_1^2\|\tilde{\boldsymbol{\omega}}\|^4 + \varepsilon^2}} - \frac{\boldsymbol{s}_1\hat{\alpha}_2^2\|\tilde{\boldsymbol{\omega}}\|^2}{\sqrt{\|\boldsymbol{s}_1\|^2\hat{\alpha}_2^2\|\tilde{\boldsymbol{\omega}}\|^2 + \varepsilon^2}}\\ &\quad - \frac{\boldsymbol{s}_1\hat{\alpha}_3^2}{\sqrt{\|\boldsymbol{s}_1\|^2\hat{\alpha}_3^2 + \varepsilon^2}} - \frac{k_3\boldsymbol{s}_1}{\sqrt{\|\boldsymbol{s}_1\|^2 + \varepsilon^2}} - k_4\boldsymbol{s}_1\end{aligned} \tag{23}$$

$$\begin{aligned}\boldsymbol{\varepsilon}_t &= -\frac{\boldsymbol{s}_2\hat{\alpha}_4^2\|\tilde{\boldsymbol{\omega}}\|^2\|\tilde{\boldsymbol{v}}\|^2}{\sqrt{\|\boldsymbol{s}_2\|^2\hat{\alpha}_4^2\|\tilde{\omega}\|^2\|\tilde{\boldsymbol{v}}\|^2 + \varepsilon^2}}\\ &\quad - \frac{\boldsymbol{s}_2\hat{\alpha}_5^2\|\tilde{\boldsymbol{\omega}}\|^2\|\tilde{\boldsymbol{r}}\|^2}{\sqrt{\|\boldsymbol{s}_2\|^2\hat{\alpha}_5^2\|\tilde{\omega}\|^2\|\tilde{\boldsymbol{r}}\|^2 + \varepsilon^2}}\\ &\quad - \frac{\boldsymbol{s}_2\hat{\alpha}_6^2\|\tilde{\boldsymbol{\omega}}\|^2}{\sqrt{\|\boldsymbol{s}_2\|^2\hat{\alpha}_6^2\|\tilde{\boldsymbol{\omega}}\|^2 + \varepsilon^2}} - \frac{\boldsymbol{s}_2\hat{\alpha}_7^2\|\tilde{\boldsymbol{v}}\|^2}{\sqrt{\|\boldsymbol{s}_2\|^2\hat{\alpha}_7^2\|\tilde{\boldsymbol{v}}\|^2 + \varepsilon^2}}\\ &\quad - \frac{\boldsymbol{s}_2\hat{\alpha}_8^2\|\tilde{\boldsymbol{r}}\|^2}{\sqrt{\|\boldsymbol{s}_2\|^2\hat{\alpha}_8^2\|\tilde{\boldsymbol{r}}\|^2 + \varepsilon^2}} - \frac{\boldsymbol{s}_2\hat{\alpha}_9^2}{\sqrt{\|\boldsymbol{s}_2\|^2\hat{\alpha}_9^2 + \varepsilon^2}}\end{aligned}$$

$$-\frac{k_7 \boldsymbol{s}_2}{\sqrt{\|\boldsymbol{s}_2\|^2+\varepsilon^2}}-k_8\boldsymbol{s}_2 \tag{24}$$

where the control parameters k_3, k_4, k_7, k_8, ε are all positive constants. Additionally, the adaptive update laws $\hat{\alpha}_i$ (i= 1, 2, 3, 4, 5, 6, 7, 8, 9) are established as:

$$\begin{cases} \dot{\hat{\alpha}}_1=\beta_1\left(\|\boldsymbol{s}_1\|\,\|\tilde{\boldsymbol{\omega}}\|^2-\gamma_1\hat{\alpha}_1\right), \\ \quad \dot{\hat{\alpha}}_2=\beta_2\left(\|\boldsymbol{s}_1\|\,\|\tilde{\boldsymbol{\omega}}\|-\gamma_2\hat{\alpha}_2\right) \\ \dot{\hat{\alpha}}_3=\beta_3\left(\|\boldsymbol{s}_1\|-\gamma_3\hat{\alpha}_3\right), \\ \quad \dot{\hat{\alpha}}_4=\beta_4\left(\|\boldsymbol{s}_2\|\,\|\tilde{\boldsymbol{\omega}}\|\,\|\tilde{\boldsymbol{v}}\|-\gamma_4\hat{\alpha}_4\right) \\ \dot{\hat{\alpha}}_5=\beta_5\left(\|\boldsymbol{s}_2\|\,\|\tilde{\boldsymbol{\omega}}\|\,\|\tilde{\boldsymbol{r}}\|-\gamma_5\hat{\alpha}_5\right), \\ \quad \dot{\hat{\alpha}}_9=\beta_9\left(\|\boldsymbol{s}_2\|-\gamma_9\hat{\alpha}_9\right) \\ \dot{\hat{\alpha}}_6=\beta_6\left(\|\boldsymbol{s}_2\|\,\|\tilde{\boldsymbol{\omega}}\|-\gamma_6\hat{\alpha}_6\right), \\ \quad \dot{\hat{\alpha}}_8=\beta_8\left(\|\boldsymbol{s}_2\|\,\|\tilde{\boldsymbol{r}}\|-\gamma_8\hat{\alpha}_8\right) \end{cases} \tag{25}$$

where $\beta_i>0$ and $\gamma_i>0$ with i = 1,2,3,4,5,6,7,8,9.

Meanwhile, the denotation of estimation errors is given as: $\tilde{\alpha}_i=\alpha_i-\hat{\alpha}_i$, i = 1,2,3,4, 5, 6, 7, 8, 9.

Remark 6: It is necessary to make a detailed description for the structure of controller (23), which mainly possesses the following salient features. i) Associated with the conclusion obtained in Remark 4, the nonlinear dynamics containing unknown inertial matrix can be approximated by adaptively estimating the parameters $\alpha_1, \alpha_2, \alpha_3$. In particular, the lumped uncertainty α_3 also consists of environmental disturbances and compensation error arising from input saturation. For these reasons, the first three items of the controller guarantee the convergence of the estimation errors. ii) As for the item $-k_3\boldsymbol{s}_1\Big/\sqrt{\|\boldsymbol{s}_1\|^2+\varepsilon^2}-k_4\boldsymbol{s}_1$, they not only contribute to the stabilization of $\boldsymbol{s}_1$, but also ensure that SMS obtains a satisfactory convergence rate in both the initial and terminal stages. iii) It should be highlighted that the introduction of the parameter ε makes the controller have capability of anti-chattering. While one caveat here is that the value of ε plays a significant role in the performance of controller. It indicates that as ε increases, the phenomenon of chattering is effectively attenuated, while the steady-state error increases accordingly. Therefore, it is necessary to carefully select ε for the overall desired performance.

Theorem 1: For the spacecraft tracking control system (11)-(12) with Assumptions 1-3, while employing the controller (23)-(24), the conclusions can be derived as:

i) The SMS (15), (16) and the estimation errors $\tilde{\alpha}_i$ (i = 1, 2, 3, 4, 5, 6, 7, 8, 9) stabilize to a neighborhood around zero as time goes to infinite.

ii) The variables $\boldsymbol{\chi}_1$ and $\boldsymbol{\chi}_2$ in the anti-saturation auxiliary system stabilize to a compact set $\Omega_2=\left\{\boldsymbol{\chi}_j\,\middle|\,\|\boldsymbol{\chi}_j\|\le\frac{\kappa_j\delta}{\kappa_j-\varpi_j}\right\}$, j = 1, 2 for $\forall t\ge 0$.

iii) The tracking errors $\tilde{\boldsymbol{q}}_v$, $\tilde{\boldsymbol{\omega}}$, $\tilde{\boldsymbol{r}}$ and $\tilde{\boldsymbol{v}}$ are capable of converging to a tiny region around the origin.

Proof: To clarify the stabilization of SMS, the first Lyapunov function is chosen as:

$$V_1=\frac{1}{2}\boldsymbol{s}_1^{\mathrm{T}}\boldsymbol{J}\boldsymbol{s}_1+\frac{1}{2}\boldsymbol{s}_2^{\mathrm{T}}m\boldsymbol{s}_2+\sum_{i=1}^{9}\frac{1}{\beta_i}\tilde{\alpha}_i^2 \tag{26}$$

Taking its time derivative and substituting Eqs. (19)-(22) yields:

$$\begin{aligned}\dot{V}_1&=\boldsymbol{s}_1^{\mathrm{T}}\boldsymbol{J}\dot{\boldsymbol{s}}_1+\boldsymbol{s}_2^{\mathrm{T}}m\dot{\boldsymbol{s}}_2-\sum_{i=1}^{9}\frac{1}{\beta_i}\tilde{\alpha}_i\dot{\hat{\alpha}}_i \\ &=\boldsymbol{s}_1^{\mathrm{T}}\Big[\boldsymbol{\varepsilon}_r-\boldsymbol{C}_r\tilde{\boldsymbol{\omega}}-\boldsymbol{n}_r+\boldsymbol{d}_r+\frac{k_1}{2}\boldsymbol{J}\left(\tilde{\boldsymbol{q}}_v^{\times}+\tilde{q}_0\boldsymbol{I}_3\right)\tilde{\boldsymbol{\omega}} \\ &\quad+\kappa_1\tanh\left(\boldsymbol{\chi}_1\right)\Big]+\boldsymbol{s}_2^{\mathrm{T}}\Big[\boldsymbol{\varepsilon}_t-m\boldsymbol{C}_t\tilde{\boldsymbol{v}}-m\boldsymbol{n}_t+\boldsymbol{d}_t+mk_2\dot{\tilde{\boldsymbol{r}}} \\ &\quad+\kappa_2\tanh\left(\boldsymbol{\chi}_2\right)\Big]-\sum_{i=1}^{9}\frac{1}{\beta_i}\tilde{\alpha}_i\dot{\hat{\alpha}}_i \\ &\le\boldsymbol{s}_1^{\mathrm{T}}\boldsymbol{\varepsilon}_r+\|\boldsymbol{s}_1\|\left(\alpha_1\|\tilde{\boldsymbol{\omega}}\|^2+\alpha_2\|\tilde{\boldsymbol{\omega}}\|+\alpha_3\right)+\boldsymbol{s}_2^{\mathrm{T}}\boldsymbol{\varepsilon}_t \\ &\quad+\|\boldsymbol{s}_2\|\left(\alpha_4\|\tilde{\boldsymbol{\omega}}\|\,\|\tilde{\boldsymbol{v}}\|+\alpha_5\|\tilde{\boldsymbol{\omega}}\|\,\|\tilde{\boldsymbol{r}}\|+\alpha_6\|\tilde{\boldsymbol{\omega}}\|+\alpha_7\|\tilde{\boldsymbol{v}}\|\right. \\ &\quad\left.+\alpha_8\|\tilde{\boldsymbol{r}}\|+\alpha_9\right)-\sum_{i=1}^{9}\frac{1}{\beta_i}\tilde{\alpha}_i\dot{\hat{\alpha}}_i\end{aligned} \tag{27}$$

While accounting for the control signals $\boldsymbol{\varepsilon}_r$, $\boldsymbol{\varepsilon}_t$ in Eqs. (26) and (27), it leads to:

$$\begin{aligned}\dot{V}_1\le&\boldsymbol{s}_1^{\mathrm{T}}\left(-\frac{\boldsymbol{s}_1\hat{\alpha}_1^2\|\tilde{\omega}\|^4}{\sqrt{\|\boldsymbol{s}_1\|^2\hat{\alpha}_1^2\|\tilde{\omega}\|^4+\varepsilon^2}}-\frac{\boldsymbol{s}_1\hat{\alpha}_2^2\|\tilde{\omega}\|^2}{\sqrt{\|\boldsymbol{s}_1\|^2\hat{\alpha}_2^2\|\tilde{\omega}\|^2+\varepsilon^2}}\right. \\ &\left.-\frac{\boldsymbol{s}_1\hat{\alpha}_3^2}{\sqrt{\|\boldsymbol{s}_1\|^2\hat{\alpha}_3^2+\varepsilon^2}}-\frac{k_3\boldsymbol{s}_1}{\sqrt{\|\boldsymbol{s}_1\|^2+\varepsilon^2}}-k_4\boldsymbol{s}_1\right) \\ &+\|\boldsymbol{s}_1\|\left(\alpha_1\|\tilde{\boldsymbol{\omega}}\|^2\right. \\ &\left.+\alpha_2\|\tilde{\boldsymbol{\omega}}\|+\alpha_3\right)+\boldsymbol{s}_2^{\mathrm{T}}\left(-\frac{\boldsymbol{s}_2\hat{\alpha}_4^2\|\tilde{\omega}\|^2\|\tilde{\boldsymbol{v}}\|^2}{\sqrt{\|\boldsymbol{s}_2\|^2\hat{\alpha}_4^2\|\tilde{\omega}\|^2\|\tilde{\boldsymbol{v}}\|^2+\varepsilon^2}}\right. \\ &-\frac{\boldsymbol{s}_2\hat{\alpha}_5^2\|\tilde{\omega}\|^2\|\tilde{\boldsymbol{r}}\|^2}{\sqrt{\|\boldsymbol{s}_2\|^2\hat{\alpha}_5^2\|\tilde{\omega}\|^2\|\tilde{\boldsymbol{r}}\|^2+\varepsilon^2}}-\frac{\boldsymbol{s}_2\hat{\alpha}_6^2\|\tilde{\omega}\|^2}{\sqrt{\|\boldsymbol{s}_2\|^2\hat{\alpha}_6^2\|\tilde{\omega}\|^2+\varepsilon^2}} \\ &-\frac{\boldsymbol{s}_2\hat{\alpha}_7^2\|\tilde{\boldsymbol{v}}\|^2}{\sqrt{\|\boldsymbol{s}_2\|^2\hat{\alpha}_7^2\|\tilde{\boldsymbol{v}}\|^2+\varepsilon^2}}-\frac{\boldsymbol{s}_2\hat{\alpha}_8^2\|\tilde{\boldsymbol{r}}\|^2}{\sqrt{\|\boldsymbol{s}_2\|^2\hat{\alpha}_8^2\|\tilde{\boldsymbol{r}}\|^2+\varepsilon^2}} \\ &\left.-\frac{\boldsymbol{s}_2\hat{\alpha}_9^2}{\sqrt{\|\boldsymbol{s}_2\|^2\hat{\alpha}_9^2+\varepsilon^2}}-\frac{k_7\boldsymbol{s}_2}{\sqrt{\|\boldsymbol{s}_2\|^2+\varepsilon^2}}-k_8\boldsymbol{s}_2\right) \\ &+\|\boldsymbol{s}_2\|\left(\alpha_4\|\tilde{\boldsymbol{\omega}}\|\,\|\tilde{\boldsymbol{v}}\|+\alpha_5\|\tilde{\boldsymbol{\omega}}\|\,\|\tilde{\boldsymbol{r}}\|+\alpha_6\|\tilde{\boldsymbol{\omega}}\|+\alpha_7\|\tilde{\boldsymbol{v}}\|\right. \\ &\left.+\alpha_8\|\tilde{\boldsymbol{r}}\|+\alpha_9\right)-\sum_{i=1}^{9}\frac{1}{\beta_i}\tilde{\alpha}_i\dot{\hat{\alpha}}_i\end{aligned} \tag{28}$$

In particular, by virtue of lemma 2, there exists an explicit inequality: $-\frac{(\delta x)^2}{\sqrt{(\delta x)^2+n^2}}\le-(\delta x)+n$, where δ is an arbitrary real number, x denotes a state variable, n stands for a nonnegative constant. Therefore, combing with Eq.(25), Eq. (28) can be further obtained as:

$$\begin{aligned}\dot{V}_1\le&\|\boldsymbol{s}_1\|\left(\alpha_1\|\tilde{\boldsymbol{\omega}}\|^2+\alpha_2\|\tilde{\boldsymbol{\omega}}\|+\alpha_3\right)-\|\boldsymbol{s}_1\|\hat{\alpha}_1\|\tilde{\omega}\|^2+\varepsilon \\ &-\|\boldsymbol{s}_1\|\hat{\alpha}_2\|\tilde{\omega}\|+\varepsilon-\|\boldsymbol{s}_1\|\hat{\alpha}_3+\varepsilon-k_3\|\boldsymbol{s}_1\|+\varepsilon \\ &-k_4\boldsymbol{s}_1^{\mathrm{T}}\boldsymbol{s}_1+\|\boldsymbol{s}_2\|\left(\alpha_4\|\tilde{\boldsymbol{\omega}}\|\,\|\tilde{\boldsymbol{v}}\|+\alpha_5\|\tilde{\boldsymbol{\omega}}\|\,\|\tilde{\boldsymbol{r}}\|+\alpha_6\|\tilde{\boldsymbol{\omega}}\|\right.\end{aligned}$$

$$
\begin{aligned}
&+\alpha_7\|\tilde{v}\|+\alpha_8\|\tilde{r}\|+\alpha_9)-\|\boldsymbol{s}_2\|\hat{\alpha}_4\|\tilde{\omega}\|\|\tilde{\boldsymbol{v}}\| \\
&-\|\boldsymbol{s}_2\|\hat{\alpha}_5\|\tilde{\omega}\|\|\tilde{\boldsymbol{r}}\|-\|\boldsymbol{s}_2\|\hat{\alpha}_6\|\tilde{\omega}\|-\|\boldsymbol{s}_2\|\hat{\alpha}_7\|\tilde{\boldsymbol{v}}\| \\
&-\|\boldsymbol{s}_2\|\hat{\alpha}_8\|\tilde{\boldsymbol{r}}\|-\|\boldsymbol{s}_2\|\hat{\alpha}_9-k_7\|\boldsymbol{s}_2\|+7\varepsilon-k_8\|\boldsymbol{s}_2\|^2 \\
&-\sum_{i=1}^{9}\frac{1}{\beta_i}\tilde{\alpha}_i\dot{\hat{\alpha}}_i \\
=&-k_3\|\boldsymbol{s}_1\|-k_4\|\boldsymbol{s}_1\|^2-k_7\|\boldsymbol{s}_2\|-k_8\|\boldsymbol{s}_2\|^2 \\
&+\sum_{i=1}^{9}\gamma_i\hat{\alpha}_i\tilde{\alpha}_i+11\varepsilon
\end{aligned}
\tag{29}
$$

At this point, notice that one of the items can be mathematically scaled as:

$$
\begin{aligned}
\gamma_i\hat{\alpha}_i\tilde{\alpha}_i&=\gamma_i\left(-\tilde{\alpha}_i^2+\alpha_i\tilde{\alpha}_i\right) \\
&\le\gamma_i\left(-\tilde{\alpha}_i^2+\frac{1}{2\iota_i}\tilde{\alpha}_i^2+\frac{\iota_i}{2}\alpha_i^2\right) \\
&=-\frac{\gamma_i\left(2\iota_i-1\right)}{2\iota_i}\tilde{\alpha}_i^2+\frac{\gamma_i\iota_i}{2}\alpha_i^2
\end{aligned}
\tag{30}
$$

with $\iota_i>0.5$ and $i=1,2,3,4,5,6,7,8,9$. Then, substituting these inequations into Eq (44), $\dot{V}_1$ can be further derived as:

$$
\begin{aligned}
\dot{V}_1&\le-k_4\|\boldsymbol{s}_1\|^2-k_8\|\boldsymbol{s}_2\|^2-\sum_{i=1}^{9}\frac{\gamma_i\left(2\iota_i-1\right)}{2\iota_i}\tilde{\alpha}_i^2 \\
&\quad+\sum_{i=1}^{9}\frac{\gamma_i\iota_i}{2}\alpha_i^2+11\varepsilon \\
&\le-\rho_1V_1-\rho_2V_1+\Delta_1+\Delta_2
\end{aligned}
\tag{31}
$$

where

$$
\rho_1=\min\left\{\frac{2k_4}{\|\boldsymbol{J}\|_{\max}},\frac{\beta_{i_1}\gamma_{i_1}\left(2\iota_{i_1}-1\right)}{\iota_{i_1}}\right\}
$$

$$
\Delta_1=\sum_{i_1=1}^{9}\frac{\gamma_{i_1}\iota_{i_1}}{2}\alpha_{i_1}^2+4\varepsilon,\quad i_1=1,2,3 \tag{32}
$$

$$
\rho_2=\min\left\{\frac{2k_8}{m},\frac{\beta_{i_2}\gamma_{i_2}\left(2\iota_{i_2}-1\right)}{\iota_{i_2}}\right\}
$$

$$
\Delta_2=\sum_{i_2=1}^{9}\frac{\gamma_{i_2}\iota_{i_2}}{2}\alpha_{i_2}^2+7\varepsilon,\quad i_2=4,5,6,7,8,9 \tag{33}
$$

As a result, it can be derived that V_1 satisfies the following inequality:

$$
0<V_1\le\frac{\Delta_j}{\rho_j}+\left(V_1\left(0\right)-\frac{\Delta_j}{\rho_j}\right)e^{-\rho_jt} \tag{34}
$$

with $j=1,2$.

Hence, it can be concluded that $\boldsymbol{s}_1$, $\boldsymbol{s}_2$ and $\tilde{\alpha}_i$ (i= 1, 2, 3, 4, 5, 6, 7, 8, 9) are all asymptotically stabilize to a tiny region containing the origin. As the time goes to infinity, $\boldsymbol{s}_1$ and $\boldsymbol{s}_2$ will converge to a residual set $\Omega_1=\left\{\boldsymbol{s}_j\,\middle|\,\|\boldsymbol{s}_j\|\le o_j\right\}$ with $o_j=\sqrt{\frac{2\Delta_j}{\rho_j}}$, $j=1,2$.

The point i) of Theorem 1 has been authenticated.

To proceed further, since the variables $\tilde{\alpha}_i$ ($i=1,2,3,4,5,6,7,8,9$) are ultimately bounded, the boundness of adaptive parameters $\hat{\alpha}_i$ can be ensured. On the other side, it has been validated that the SMS $\boldsymbol{s}_1$ and $\boldsymbol{s}_2$ are bounded, so that the control signal $\boldsymbol{\varepsilon}_r$ and $\boldsymbol{\varepsilon}_t$ must be bounded. Based on this conclusion, two nonnegative constants ϖ_1,ϖ_2 are defined as $\|\mathrm{sat}\left(\boldsymbol{\varepsilon}_r\right)-\boldsymbol{\varepsilon}_r\|\le\varpi_1$ and $\|\mathrm{sat}\left(\boldsymbol{\varepsilon}_t\right)-\boldsymbol{\varepsilon}_t\|\le\varpi_2$, respectively. To corroborate the stability of anti-saturation auxiliary system, the Lyapunov function is chosen as:

$$
V_2=\frac{1}{2}k_2\boldsymbol{\chi}_1^{\mathrm{T}}\boldsymbol{\chi}_1+\frac{1}{2}k_6\boldsymbol{\chi}_2^{\mathrm{T}}\boldsymbol{\chi}_2 \tag{35}
$$

Taking the dynamics (17) and (18) into consideration, the time differential of V_2 is derived as:

$$
\begin{aligned}
\dot{V}_2&=k_2\boldsymbol{\chi}_1^{\mathrm{T}}\dot{\boldsymbol{\chi}}_1+k_6\boldsymbol{\chi}_2^{\mathrm{T}}\dot{\boldsymbol{\chi}}_2 \\
&=\boldsymbol{\chi}_1^{\mathrm{T}}\boldsymbol{\varphi}^{-1}\boldsymbol{J}^{-1}\left[-\kappa_1\tanh\left(\boldsymbol{\chi}_1\right)+\mathrm{sat}\left(\boldsymbol{\varepsilon}_r\right)-\boldsymbol{\varepsilon}_r\right] \\
&\quad+\boldsymbol{\chi}_2^{\mathrm{T}}\boldsymbol{\varphi}^{-1}m^{-1}\left[-\kappa_2\tanh\left(\boldsymbol{\chi}_2\right)+\mathrm{sat}\left(\boldsymbol{\varepsilon}_t\right)-\boldsymbol{\varepsilon}_t\right]
\end{aligned}
\tag{36}
$$

On the basis of Lemma 1, the following inequalities hold:

$$
\begin{aligned}
-\kappa_1\boldsymbol{\chi}_1^{\mathrm{T}}\tanh\left(\boldsymbol{\chi}_1\right)&\le-\kappa_1\left\|\boldsymbol{\chi}_1\right\|+\kappa_1\delta \\
-\kappa_2\boldsymbol{\chi}_2^{\mathrm{T}}\tanh\left(\boldsymbol{\chi}_2\right)&\le-\kappa_2\left\|\boldsymbol{\chi}_2\right\|+\kappa_2\delta
\end{aligned}
\tag{37}
$$

By invoking the inequalities (37) into (36), the differential of V_2 becomes:

$$
\begin{aligned}
\dot{V}_2&\le\left\|\boldsymbol{\varphi}^{-1}\boldsymbol{J}^{-1}\right\|\left[-\kappa_1\left\|\boldsymbol{\chi}_1\right\|+\kappa_1\delta+\varpi_1\left\|\boldsymbol{\chi}_1\right\|\right] \\
&\quad+m^{-1}\left\|\boldsymbol{\varphi}^{-1}\right\|\left[-\kappa_2\left\|\boldsymbol{\chi}_2\right\|+\kappa_2\delta+\varpi_2\left\|\boldsymbol{\chi}_2\right\|\right] \\
&=\left\|\boldsymbol{\varphi}^{-1}\boldsymbol{J}^{-1}\right\|\left[\kappa_1\delta-\left(\kappa_1-\varpi_1\right)\left\|\boldsymbol{\chi}_1\right\|\right] \\
&\quad+m^{-1}\left\|\boldsymbol{\varphi}^{-1}\right\|\left[\kappa_2\delta-\left(\kappa_2-\varpi_2\right)\left\|\boldsymbol{\chi}_2\right\|\right]
\end{aligned}
\tag{38}
$$

To conclude, only if the parameters κ_1,κ_2 are designed to satisfy $\kappa_1>\varpi_1$ and $\kappa_2>\varpi_2$, respectively, the auxiliary variable $\boldsymbol{\chi}_1$ and $\boldsymbol{\chi}_2$ will be restrained in the compact set $\Omega_2=\left\{\boldsymbol{\chi}_j\,\middle|\,\left\|\boldsymbol{\chi}_j\right\|\le\frac{\kappa_j\delta}{\kappa_j-\varpi_j}\right\}$, $j=1,2$ for $\forall t\ge0$, so that point ii) is authenticated.

For the purpose of verifying the convergence of the tracking errors, the Lyapunov function is selected as:

$$
V_3=\tilde{\boldsymbol{q}}_v^{\mathrm{T}}\tilde{\boldsymbol{q}}_v+\left(1-\tilde{q}_0\right)^2+\frac{1}{2}\tilde{\boldsymbol{r}}^{\mathrm{T}}\tilde{\boldsymbol{r}} \tag{39}
$$

Then, in light of Remark 4, V_3 satisfies the following inequality:

$$
V_3\le\tilde{\boldsymbol{q}}_v^{\mathrm{T}}\tilde{\boldsymbol{q}}_v+4+\frac{1}{2}\tilde{\boldsymbol{r}}^{\mathrm{T}}\tilde{\boldsymbol{r}} \tag{40}
$$

With the property of $q_0^2+\boldsymbol{q}_v^{\mathrm{T}}\boldsymbol{q}_v=1$ and differentiating V_3 with respect to Eqs. (15) and (16) yield:

$$
\begin{aligned}
\dot{V}_3&=-2\dot{\tilde{q}}_0+\tilde{\boldsymbol{r}}^{\mathrm{T}}\dot{\tilde{\boldsymbol{r}}} \\
&=\tilde{\boldsymbol{q}}_v^{\mathrm{T}}\left(\boldsymbol{s}_1-k_1\tilde{\boldsymbol{q}}_v+k_2\tanh\left(\boldsymbol{\chi}_1\right)\right) \\
&\quad+\tilde{\boldsymbol{r}}^{\mathrm{T}}\left(\boldsymbol{s}_2-k_5\tilde{\boldsymbol{r}}+k_6\tanh\left(\boldsymbol{\chi}_2\right)-\boldsymbol{C}_t\tilde{\boldsymbol{r}}\right) \\
&\le-\left(k_1-\frac{1}{2}\right)\left(\tilde{\boldsymbol{q}}_v^{\mathrm{T}}\tilde{\boldsymbol{q}}_v+4\right)+o_1^2+k_2^2+2\left(k_1-\frac{1}{2}\right)
\end{aligned}
$$

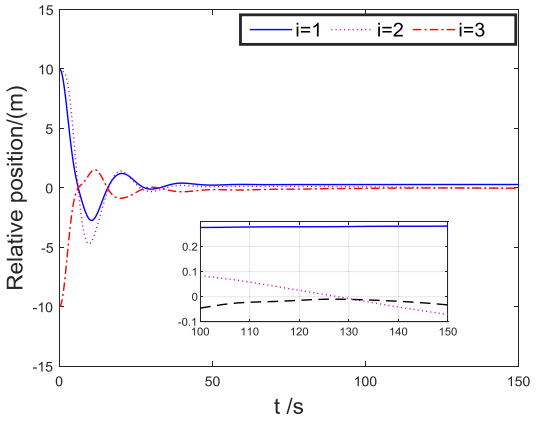

FIGURE 1. Curves of relative position.

$$
\begin{aligned}
&-\left(k_5+\|\boldsymbol{C}_t\|-\frac{1}{2}\right)\|\tilde{\boldsymbol{r}}\|^2+o_2^2+k_6^2\\
&\leq-\left(k_1+2k_5+2\|\boldsymbol{C}_t\|-\frac{3}{2}\right)V_2+o_1^2+k_2^2\\
&\quad+2\left(k_1-\frac{1}{2}\right)+o_2^2+k_6^2 \qquad (41)
\end{aligned}
$$

Thus, V_3 will converge to a small region asymptotically. Observing the definition of V_3, it concludes that tracking errors $\tilde{\boldsymbol{q}}_v$ and $\tilde{\boldsymbol{r}}$ will converge to a small region asymptotically, which can be recorded as $\Omega_3 = \left\{\tilde{\boldsymbol{q}}_v \,|\, \|\tilde{\boldsymbol{q}}_v\| \leq o_3, \tilde{\boldsymbol{r}} \,|\, \|\tilde{\boldsymbol{r}}\| \leq o_4 \right\}$.

Considering the SMSs constructed in Eqs. (15) and (16), due to bounded $\boldsymbol{s}_j$ and $\boldsymbol{\chi}_j, j = 1, 2$ and the foregoing analysis, we have:

$$
\begin{aligned}
\tilde{\omega}_i &\leq o_1 - k_1\tilde{q}_{vi} + k_2\tanh(\chi_{1i})\\
&\leq o_1 + k_1|\tilde{q}_{vi}| + k_2|\tanh(\chi_{1i})|\\
&\leq o_1 + k_1 o_3 + k_2\tanh\left(\frac{\kappa_1\delta}{\kappa_1-\varpi_1}\right) = o_5 \qquad (42)\\
\tilde{v}_i &\leq o_2 - k_5\tilde{r}_i + k_6\tanh(\chi_{2i})\\
&\leq o_2 + k_5|\tilde{r}_i| + k_6|\tanh(\chi_{2i})|\\
&\leq o_2 + k_5 o_4 + k_6\tanh\left(\frac{\kappa_2\delta}{\kappa_2-\varpi_2}\right) = o_6 \qquad (43)
\end{aligned}
$$

Naturally, the boundness of tracking errors $\tilde{\boldsymbol{\omega}}$ and $\tilde{\boldsymbol{v}}$ can be warranted from mathematical proof above with $\Omega_4 = \{\tilde{\boldsymbol{\omega}} \,|\, \|\tilde{\boldsymbol{\omega}}\| \leq o_5,\ \tilde{\boldsymbol{v}} \,|\, \|\tilde{\boldsymbol{v}}\| \leq o_6 \}$.

Consequently, the Theorem 1 has been finally proved.

IV. SIMULATION RESULTS

In this section, a simulation example of spacecraft rendezvous is provided to verify the characteristic of proposed controller. After given orbit information and spacecraft parameters, we set the position and attitude of the target and record the trajectory of the pursuer under designed control signal. According to the obtained results, the transient and steady-state performance of the control system are analyzed and compared in detail.

TABLE 1. Orbit information and spacecraft parameters [1].

Parameter	Value	Unit
Gravitational constant, μ	6.371	km
Eccentricity, e	0.3	—
Radius of the Earth, R_E	6371	km
Perigee altitude, r_{pa}	400	km
Initial true anomaly, $v(0)$	12	degrees
Inertial matrix, $\boldsymbol{J}$	$\mathrm{diag}(21,18,16)$	$\mathrm{kg}\cdot\mathrm{m}^2$
Inertial matrix, $\boldsymbol{J}_t$	$\mathrm{diag}(26.5,16.02,21.984)$	$\mathrm{kg}\cdot\mathrm{m}^2$
Mass, m	95	kg
Mass, m_t	145	kg

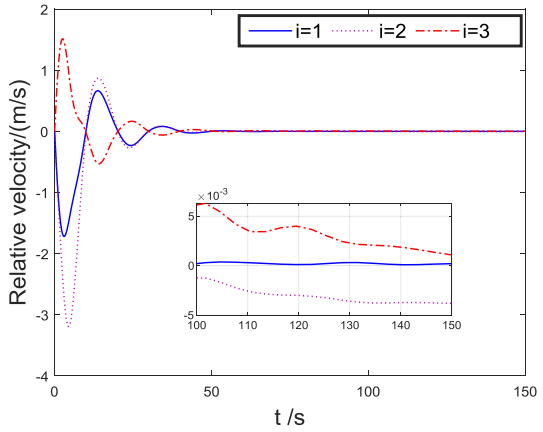

FIGURE 2. Curves of relative velocity.

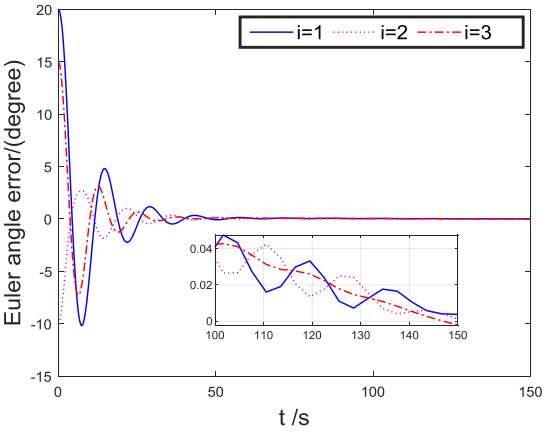

FIGURE 3. Curves of Euler angle error.

The input saturation constraints are set as: The reference position of the target spacecraft is given as [1]:

$$
\boldsymbol{r}_t = [r_t, 0, 0]^{\mathrm{T}}, \quad r_t = \frac{a\left(1-e^2\right)}{1+e\cos v} \qquad (44)
$$

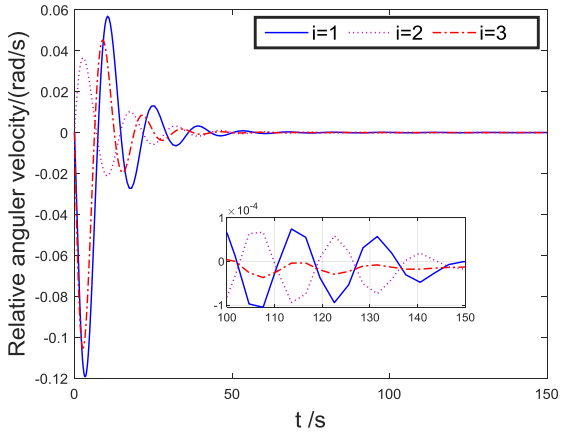

FIGURE 4. Curves of relative angular velocity.

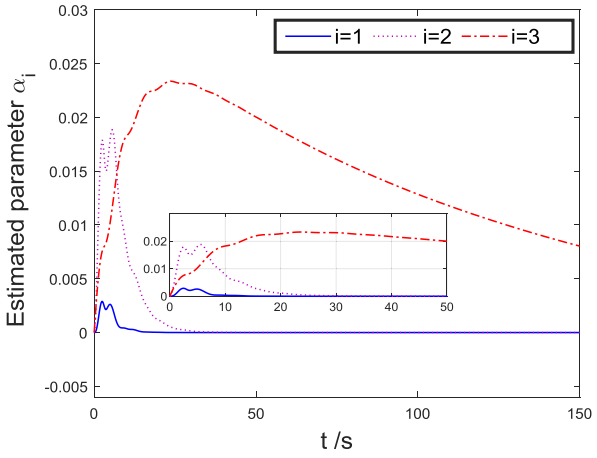

FIGURE 5. Estimated parameter in attitude dynamics.

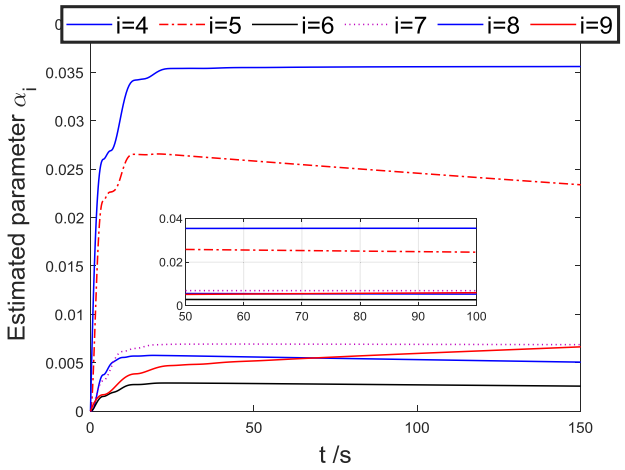

FIGURE 6. Estimated parameters in position dynamics.

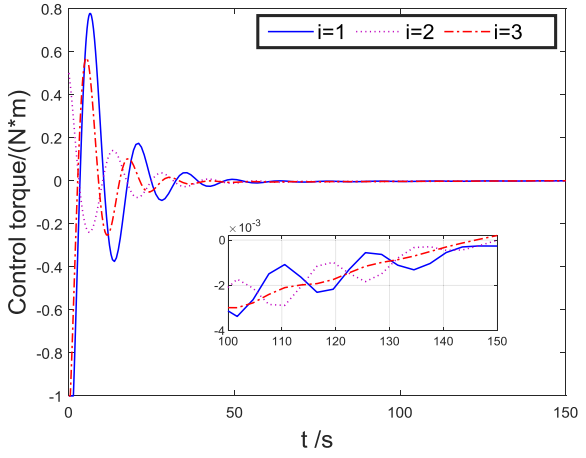

FIGURE 7. Control torque of position subsystem.

where $a = R_E + \frac{r_{pa}}{1-e}$ represents the semimajor axis and the parameter v satisfies:

$$\dot{v} = \frac{n\left(1+e\cos v\right)^2}{\left(1-e^2\right)^{\frac{3}{2}}}, \quad \ddot{v} = \frac{2n^2 e\left(1+e\cos v\right)^3 \sin v}{\left(1-e^2\right)^3} \tag{45}$$

where $n = \sqrt{u/a^3}$. Afterwards, the rendezvous position is set as $\boldsymbol{\delta}_t = [0, 5, 0]^{\mathrm{T}}$ in the body coordinate frame of the target. The disturbance torques and the initial conditions are defined as:

$$\begin{aligned}
\boldsymbol{\tau}_d &= 0.001 \times \left(0.5 + \sin\left(\frac{\pi}{100}t\right) + \cos\left(\frac{\pi}{100}t\right)\right) \\
&\quad \times [1; 1; 1]^{\mathrm{T}}\,\mathrm{N}\cdot\mathrm{m} \\
\boldsymbol{f}_d &= 0.002 \times \left(0.5 + \cos\left(\frac{\pi}{100}t\right) + \sin\left(\frac{\pi}{100}t\right)\right) \\
&\quad \times [1; 1; 1]^{\mathrm{T}}\,\mathrm{N}\cdot\mathrm{m} \\
\Theta\left(0\right) &= [18.5 - 9.3\ 14.02]^{\mathrm{T}}\,\mathrm{deg}, \quad \tilde{\boldsymbol{\omega}} = [000]^{\mathrm{T}}\,\mathrm{rad/s} \\
\tilde{\boldsymbol{r}}\left(0\right) &= [10, 10, -10]^{\mathrm{T}}\,\mathrm{m}, \quad \tilde{\boldsymbol{v}}\left(0\right) = [000]^{\mathrm{T}}\,\mathrm{m/s}
\end{aligned} \tag{46}$$

The control parameters are selected as follows: $k_1 = 2$, $k_2 = 0.1$, $\kappa_1 = 2$, $k_3 = 4$, $k_4 = 0.5, k_5 = 0.5$, $k_6 = 0.001$, $\kappa_2 = 2$, $k_7 = 0.5$, $k_8 = 20$, $\varepsilon = 0.001$, $\beta_1 = 10$, $\gamma_1 = 1$, $\beta_2 = 5$, $\gamma_2 = 1$, $\beta_3 = 0.1$, $\gamma_3 = 1$, $\beta_4 = 0.01$, $\gamma_4 = 1$, $\beta_5 = 0.01$, $\gamma_5 = 1$, $\beta_6 = 0.01$, $\gamma_6 = 1$, $\beta_7 = 0.001$, $\gamma_7 = 1$, $\beta_8 = 0.001$, $\gamma_8 = 1$, $\beta_9 = 0.001$, $\gamma_9 = 1$. The simulation results are shown in Figures 1-8. Figures. 1-2 illustrate the curves of relative position tracking errors and relative attitude tracking errors, respectively. It can be found that relative position tracking errors will converge to a tiny set within 0.3 at about 50s, the relative velocity converge to a smaller range also at about 50s. Then the curves of velocity tracking errors can be found in Figures 3-4. Observing Figures 3-4, it can be concluded that the Euler angle errors will close to the origin within 50s, the relative angular velocity errors are more closer to the origin at about 50s. Thus, it is indicated that the trajectory tracking of the pursuer spacecraft is completed at about 50s, while all the steady-state errors can be restricted within a very small range within 0.3. Figures 5-6 reflect the variation of the adaptive estimation values, which is utilized to approximate the uncertain dynamics caused by the time-varying inertial parameters. Their curves obviously tend to converge toward a corresponding constant. Subsequently, Figures 7-8 display

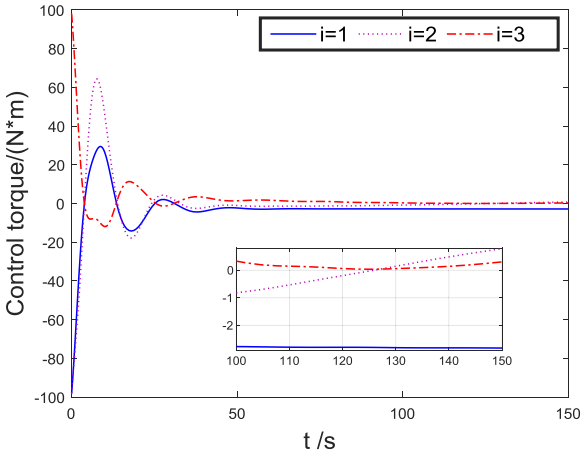

FIGURE 8. Control torque of attitude subsystem.

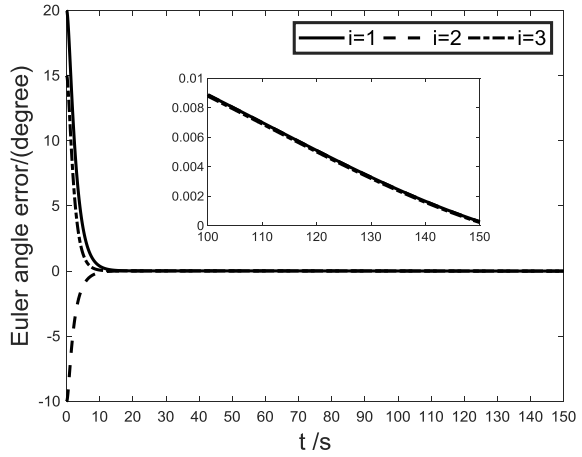

FIGURE 9. Curves of Euler angle error of [1].

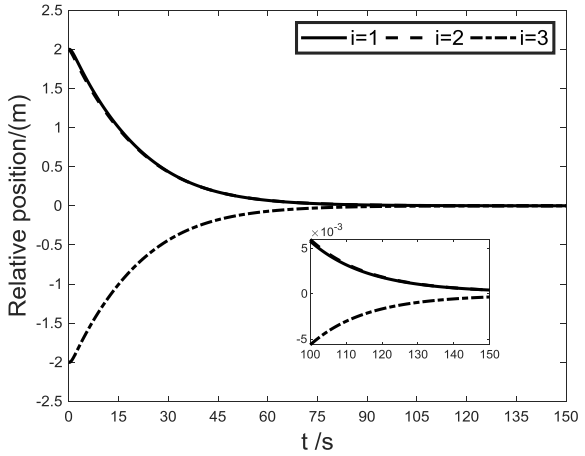

FIGURE 10. Curves of relative position of [1].

the signal waveforms of control torques, while saturation nonlinearity is imposed on the developed controller. It can be observed the control torque of position subsystem and attitude subsystem are limited to ± 1 N· m and ± 100 N· m, respectively.

To obtain better collaboration of the proposed method's efficiency, a comparative simulation example is presented here. The controller presented in [1] is applied for illustration. The basic simulation parameters are inherited from this reference. When we impose the same saturation constraints, the system will become unstable. Thus, we simulate the example without consideration of input saturation. Partial of the simulation results are presented in Figs. 9-10. Fig. 9 presented the relative attitude while Fig. 10 depicts the relative position. Obviously, the proposed method in this paper possesses longer settling time and more chattering in the attitude control aspect. However, better control performance is achieved in the position control aspect.

V. CONCLUSION

This paper focuses on the trajectory tracking control for the spacecraft rendezvous maneuver suffering from input saturation and system parameter uncertainties. The SMC-based adaptive robust algorithm is constructed to achieve the attitude and position tracking of the pursuer spacecraft. In particular, a novel anti-saturation auxiliary system is utilized to remedy the nonlinear restraint arising from the actuator saturation. In consideration of the unavailable inertial information, adaptive approximation is adopted to intensify the robustness of the controller against uncertainty. The rigorous mathematical derivation concludes that the tracking errors and estimation errors stabilize to a residual set around zero as time goes to infinite. The results of a simulation experiment confirm the conclusion and fully demonstrated the superior performance of the proposed controller.

REFERENCES

[1] Z. Shi, C. Deng, S. Zhang, Y. Xie, H. Cui, and Y. Hao, "Hyperbolic tangent function-based finite-time sliding mode control for spacecraft rendezvous maneuver without chattering," *IEEE Access*, vol. 8, pp. 60838–60849, 2020, doi: 10.1109/ACCESS.2020.2983316.

[2] B. Huang, A.-J. Li, Y. Guo, and C.-Q. Wang, "Fixed-time attitude tracking control for spacecraft without unwinding," *Acta Astronautica*, vol. 151, pp. 818–827, Oct. 2018, doi: 10.1016/j.actaastro.2018.04.041.

[3] J. Zenteno-Torres, J. Cieslak, D. Henry, and J. Davila, "A tracking backstepping sliding-mode control for spacecraft rendezvous with a passive target," in *Proc. UKACC 12th Int. Conf. Control (CONTROL)*, Sheffield, U.K., Sep. 2018, pp. 69–74, doi: 10.1109/CONTROL.2018.8516895.

[4] L. Shuhao and L. Zheng, "Frequency shaping backstepping robust attitude maneuver of flexible spacecraft," in *Proc. IEEE Int. Conf. Mechatronics, Robot. Automat. (ICMRA)*, Hefei, China, May 2018, pp. 42–46, doi: 10.1109/ICMRA.2018.8490555.

[5] X. Cao, P. Shi, Z. Li, and M. Liu, "Neural-network-based adaptive backstepping control with application to spacecraft attitude regulation," *IEEE Trans. Neural Netw. Learn. Syst.*, vol. 29, no. 9, pp. 4303–4313, Sep. 2018, doi: 10.1109/TNNLS.2017.2756993.

[6] W. Liu, Y. Geng, B. Wu, and D. Wang, "Neural-network-based adaptive event-triggered control for spacecraft attitude tracking," *IEEE Trans. Neural Netw. Learn. Syst.*, vol. 31, no. 10, pp. 4015–4024, Oct. 2020, doi: 10.1109/TNNLS.2019.2951732.

[7] Z. Wang, Q. Li, and S. Li, "Adaptive integral-type terminal sliding mode fault tolerant control for spacecraft attitude tracking," *IEEE Access*, vol. 7, pp. 35195–35207, 2019, doi: 10.1109/ACCESS.2019.2901966.

[8] Z. Wang, Q. Li, S. Jiang, and S. Li, "Finite-time fault tolerant control for spacecraft attitude systems based adding a power integrator approach," in *Proc. Chin. Control Decis. Conf. (CCDC)*, Shenyang, China, Jun. 2018, pp. 1789–1794, doi: 10.1109/CCDC.2018.8407417.

[9] K. Xia and Y. Zou, "Adaptive saturated fault-tolerant control for spacecraft rendezvous with redundancy thrusters," *IEEE Trans. Control Syst. Technol.*, vol. 29, no. 2, pp. 502–513, Mar. 2021, doi: 10.1109/TCST.2019.2950399.

[10] B. Huang, A.-J. Li, Y. Guo, and C.-Q. Wang, "Rotation matrix based finite-time attitude synchronization control for spacecraft with external disturbances," *ISA Trans.*, vol. 85, pp. 141–150, Feb. 2019, doi: 10.1016/j.isatra.2018.10.027.

[11] N. Latifu, Z. Song, C. Duan, Z. Li, H. Su, Q. Wu, and X. Liu, "Distributed full order sliding mode control for finite-time attitude synchronization and tracking of spacecraft," in *Proc. 37th Chin. Control Conf. (CCC)*, Wuhan, China, Jul. 2018, pp. 664–669, doi: 10.23919/ChiCC.2018.8483601.

[12] W. Deng and J. Yao, "Extended-state-observer-based adaptive control of electrohydraulic servomechanisms without velocity measurement," *IEEE/ASME Trans. Mechatronics*, vol. 25, no. 3, pp. 1151–1161, Jun. 2020.

[13] C. Zhu, B. Huang, B. Zhou, Y. Su, and E. Zhang, "Adaptive model-parameter-free fault-tolerant trajectory tracking control for autonomous underwater vehicles," *ISA Trans.*, Jan. 2021, doi: 10.1016/j.isatra.2020.12.059.

[14] B. Huang, B. Zhou, S. Zhang, and C. Zhu, "Adaptive prescribed performance tracking control for underactuated autonomous underwater vehicles with input quantization," *Ocean Eng.*, vol. 221, Feb. 2021, Art. no. 108549.

[15] Z. Chen, F. Huang, W. Chen, J. Zhang, W. Sun, J. Chen, J. Gu, and S. Zhu, "RBFNN-based adaptive sliding mode control design for delayed nonlinear multilateral telerobotic system with cooperative manipulation," *IEEE Trans. Ind. Informat.*, vol. 16, no. 2, pp. 1236–1247, Feb. 2020.

[16] Y. Zhang, Q. Zhang, J. Zhang, and Y. Wang, "Sliding mode control for fuzzy singular systems with time delay based on vector integral sliding mode surface," *IEEE Trans. Fuzzy Syst.*, vol. 28, no. 4, pp. 768–782, Apr. 2020.

[17] Q. Li, J. Yuan, B. Zhang, and H. Wang, "Artificial potential field based robust adaptive control for spacecraft rendezvous and docking under motion constraint," *ISA Trans.*, vol. 95, pp. 173–184, Dec. 2019.

[18] Y.-Y. Wu, Y. Zhang, and A.-G. Wu, "Attitude tracking control for rigid spacecraft with parameter uncertainties," *IEEE Access*, vol. 8, pp. 38663–38672, 2020, doi: 10.1109/ACCESS.2020.2974572.

[19] J. Bae and Y. Kim, "Adaptive controller design for spacecraft formation flying using sliding mode controller and neural networks," *J. Franklin Inst.*, vol. 349, no. 2, pp. 578–603, Mar. 2012.

[20] L. Sun, W. He, and C. Sun, "Adaptive fuzzy relative pose control of spacecraft during rendezvous and proximity maneuvers," *IEEE Trans. Fuzzy Syst.*, vol. 26, no. 6, pp. 3440–3451, Dec. 2018, doi: 10.1109/TFUZZ.2018.2833028.

[21] Y. Wang and H. Ji, "Input-to-state stability-based adaptive control for spacecraft fly-around with input saturation," *IET Control Theory Appl.*, vol. 14, no. 10, pp. 1365–1374, Jul. 2020, doi: 10.1049/iet-cta.2019.0634.

[22] Y. Guo, B. Huang, S. Wang, A.-J. Li, and C.-Q. Wang, "Adaptive finite-time control for attitude tracking of spacecraft under input saturation," *J. Aerosp. Eng.*, vol. 31, no. 2, Mar. 2018, Art. no. 04017086.

[23] Z. Ning, C. Xiaodong, X. Yuanqing, H. Jie, and W. Qiping, "Quaternion-based fault-tolerant control design for spacecraft attitude stabilization: An anti-saturation method," in *Proc. Chin. Control Conf. (CCC)*, Guangzhou, China, Jul. 2019, pp. 2558–2563, doi: 10.23919/ChiCC.2019.8866098.

[24] N. Zhou, Y. Kawano, and M. Cao, "Neural network-based adaptive control for spacecraft under actuator failures and input saturations," *IEEE Trans. Neural Netw. Learn. Syst.*, vol. 31, no. 9, pp. 3696–3710, Sep. 2020, doi: 10.1109/TNNLS.2019.2945920.

[25] T. Ye and C. Yuanli, "Quaternion based sliding mode attitude control design for spacecraft," in *Proc. 3rd IEEE Int. Conf. Control Sci. Syst. Eng. (ICCSSE)*, Beijing, China, Aug. 2017, pp. 110–114, doi: 10.1109/CCSSE.2017.8087905.

[26] M. D. Shuster, "A survey of attitude representations," *Navigation*, vol. 8, no. 9, pp. 439–517, 1993.

[27] M. J. Sidi, *Spacecraft Dynamics and Control: A Practical Engineering Approach*. Cambridge, U.K.: Cambridge Univ. Press, 1997.

[28] K. Esfandiari, F. Abdollahi, and H. A. Talebi, "Adaptive control of uncertain nonaffine nonlinear systems with input saturation using neural networks," *IEEE Trans. Neural Netw. Learn. Syst.*, vol. 26, no. 10, pp. 2311–2322, Oct. 2015.

[29] W. Deng and J. Yao, "Asymptotic tracking control of mechanical servosystems with mismatched uncertainties," *IEEE/ASME Trans. Mechatronics*, early access, Oct. 30, 2020, doi: 10.1109/TMECH.2020.3034923.

[30] X. Wu, W. Bai, Y. Xie, X. Sun, C. Deng, and H. Cui, "A hybrid algorithm of particle swarm optimization, metropolis criterion and RTS smoother for path planning of UAVs," *Appl. Soft Comput.*, vol. 73, pp. 735–747, Dec. 2018.

[31] Q. Hu, L. Xiao, and C. Wang, "Adaptive fault-tolerant attitude tracking control for spacecraft with time-varying inertia uncertainties," *Chin. J. Aeronaut.*, vol. 32, no. 3, pp. 674–687, Mar. 2019.

ZONGLING LI is currently pursuing the Ph.D. degree with the School of Information and Electronics, Beijing Institute of Technology, Beijing, China. He is currently a Senior Engineer with the Institute of Spacecraft System Engineering. His research interests include satellite systems design, space-borne computer design, and high-speed radar signal processing.

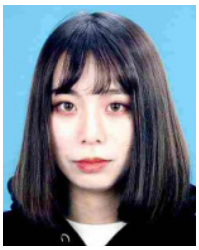

GANXIN YU was born in Harbin, China. She is currently pursuing the bachelor's degree in aircraft design and engineering with Harbin Engineering University. Her research interests include spacecraft dynamics, fault-tolerant control, and sliding mode control.

QINGJUN ZHANG research interests include spacecraft dynamics, finite-time control, formation control, and sliding mode control.

SHUO SONG is currently pursuing the bachelor's degree in automation with Harbin Engineering University. His research interests include nonlinear control, path planning, and event-triggered control.

HONGTAO CUI received the bachelor's and master's degrees with Heilongjiang University, in 2013 and 2016, respectively. He is currently pursuing the Ph.D. degree with Harbin Engineering University. His research interests include spacecraft dynamics modeling and control and multibody dynamics modeling and control.